

Model-agnostic explainable artificial intelligence for object detection in image data

Milad Moradi*

AI Research, Tricentis, Vienna, Austria

m.moradi-vastegani@tricentis.com

Ke Yan

AI Research, Tricentis, Sydney, Australia

k.yan@tricentis.com

David Colwell

AI Research, Tricentis, Sydney, Australia

d.colwell@tricentis.com

Matthias Samwald

Institute of Artificial Intelligence, Center for Medical Statistics, Informatics, and Intelligent Systems,
Medical University of Vienna, Vienna, Austria

matthias.samwald@meduniwien.ac.at

Rhona Asgari

AI Research, Tricentis, Vienna, Austria

r.asgari@tricentis.com

* Corresponding author. **Postal address:** Tricentis GmbH, Leonard-Bernstein-Straße 10, 1220 Vienna, Austria.

Abstract

In recent years, deep neural networks have been widely used for building high-performance Artificial Intelligence (AI) systems for computer vision applications. Object detection is a fundamental task in computer vision, which has been greatly progressed through developing large and intricate deep learning models. However, the lack of transparency is a big challenge that may not allow the widespread adoption of these models. Explainable artificial intelligence is a field of research where methods are developed to help users understand the behavior, decision logics, and vulnerabilities of AI-based systems. Black-box explanation refers to explaining decisions of an AI system without having access to information about its architecture, internals, and parameters. Previously, few explanation methods were developed for object detection, based on the idea of random masks. However, random masks may raise some issues regarding the actual importance of pixels within an image. In this paper, we design and implement a black-box explanation method named **B**lack-box **O**bject **D**etection **E**xplanation by **M**asking (BODEM) through adopting a new masking approach for AI-based object detection systems. We propose local and distant masking to generate multiple versions of an input image. Local masks are used to disturb pixels within a target object to figure out how the object detector reacts to these changes, while distant masks are used to assess how the detection model's decisions are affected by disturbing pixels outside the object.. A saliency map is then created by estimating the importance of pixels through measuring the difference between the detection output before and after masking. Finally, a heatmap is created that visualizes how important pixels within the input image are to the detected objects (based on the importance values estimated within the saliency map). The experimentations on various object detection datasets and models showed that BODEM can be effectively used to explain the behavior of object detectors and reveal their vulnerabilities. This makes BODEM suitable for explaining and validating AI based object detection systems in black-box software testing scenarios. Furthermore, we conducted data augmentation experiments that showed local masks produced by BODEM can be used for further training the object detectors and improve their detection accuracy and robustness.

Keywords: Explainable artificial intelligence, Deep learning, Computer vision, Object detection, Local masking, Software testing

1. Introduction and background

Artificial Intelligence (AI) and Machine Learning (ML) methods have been widely used in recent years for building intelligent systems, which can accurately perform automatic tasks that require human intelligence. Deep Neural Networks (DNNs) have had a major contribution in the success of AI systems, due to their great abilities in capturing complex data relationships. DNNs trained on sufficiently large datasets can then be used as either high-performance generative or discriminative ML models. A generative ML model captures the joint probability of the data and the target in a supervised scenario, or the distribution of the data itself in an unsupervised scenario. Generative models can be used to extract patterns from large datasets or to generate new samples that look like real data. On the other hand, a discriminative ML model captures the conditional probability of the data and the target. Discriminative modelling is usually used to build predictive ML models that perform common predictive tasks such as classification and regression. Both generative and discriminative approaches have found various applications in pattern recognition, computer vision, natural language processing, speech recognition, and recommender systems ([Weibo Liu et al., 2017](#)).

A DNN consists of a hierarchical architecture of layers, with each layer containing multiple non-linear processing units. When training a DNN, lower layers (i.e. layers that are closer to the input) usually learn simpler data relationships and pass them to the next layers. As the input passes through a DNN's layers, more complex patterns are learned, building on simpler patterns learned by the previous layers. Upper layers of a DNN, which are closer to the final output, usually act as functions that approximate the target output that is specified by the task at hand. Multi-layer perceptrons, deep belief networks, autoencoders, Convolutional Neural Networks (CNNs), Recurrent Neural Networks (RNNs), and transformers are the most commonly used DNN architectures with various applications in image, text, time series, and tabular data processing ([Khamparia & Singh, 2019](#); [LeCun, Bengio, & Hinton, 2015](#); [Weibo Liu et al., 2017](#)).

CNN is a popular DNN architecture inspired by the organization of the natural visual perception of living creatures ([Gu et al., 2018](#)). CNNs can be ideal models for extracting patterns from multi-dimensional data with grid-like topology, e.g. images and videos. Convolutional layers in a CNN convolve their input with trainable filters at all possible receptive fields, resulting in local feature maps. Using pooling layers, subsampling is then performed on the feature maps to reduce their size. As the input passes through multiple convolutional and subsampling layers, higher level transformations of the input are constructed. Finally, after rasterizing, which represents the final feature map as a one-dimensional vector, the output of the CNN is fed into one or more fully-connected layers to produce the final output.

CNNs have various applications in computer vision and image processing. They can effectively help AI systems gain high-level understanding from digital images and detect complex structures. A CNN is composed of simple but non-linear modules, which learn multiple levels of abstraction in multiple layers of the neural network. The input of the first layer comes in the form of arrays of pixel values in different RGB channels, or other colour models. The representations learned by the first layer typically encode the presence or absence of edges with particular orientation at specific locations in the image. The subsequent layers usually detect particular combinations of edges and encode motifs into feature maps, and then identify parts of familiar objects as a result of combining motifs. Finally, the last layers detect objects through assembling those parts identified by the previous layers (LeCun et al., 2015).

Object detection is a fundamental task in image processing, whose goal is to localize and classify objects in an image (Zaidi et al., 2022). Object detection can provide essential information for semantic understanding of images and videos, which has applications in autonomous driving, image classification, face recognition, and other related tasks (Zhao, Zheng, Xu, & Wu, 2019). With the emergence of DNNs, we have witnessed considerable performance improvement in computer vision applications, especially object detection. CNNs typically form the backbone of object detection systems and serve as feature detectors (Jiao et al., 2019). Regions with CNN (R-CNN) (Girshick, Donahue, Darrell, & Malik, 2014), Fast R-CNN (Girshick, 2015), Faster R-CNN (Ren, He, Girshick, & Sun, 2015), Mask R-CNN (He, Gkioxari, Dollár, & Girshick, 2017), You Only Look Once (YOLO) (Redmon, Divvala, Girshick, & Farhadi, 2016), and Single-Shot Detector (SSD) (Wei Liu et al., 2016) are among the most popular object detection models.

In spite of deep learning methods' impressive success, the lack of interpretability has been a barrier to the widespread adoption of these methods, especially in mission critical applications (Guidotti et al., 2018). In order to trust an ML model, users need to be able to explain or interpret what the model has learned (Murdoch, Singh, Kumbier, Abbasi-Asl, & Yu, 2019). It is easier to trust an ML model's decisions, detect its potential biases, take actions to refine it, and optimize its performance when we have a clear understanding of the model, its behaviour, and its vulnerabilities (Moradi & Samwald, 2021b, 2021c, 2022a).

Explainable AI (XAI) is a field of research where methods are studied and developed to provide users with the ability of understanding, explaining, and interpreting AI and ML systems (Adadi & Berrada, 2018). There are several examples of black-box AI models whose decisions were revealed to be biased or unfair after explaining them (Guidotti et al., 2018). In computer vision, XAI has also helped to discover biases and failure points of DL models utilized for object detection and classification (Freitas, 2014; Ribeiro, Singh, & Guestrin, 2016). XAI methods for

computer vision can be divided into two categories, i.e. white-box and black-box, based on their access to the DL model's internals. White-box methods have access to information about the underlying DL network, such as its architecture, loss function, activation functions, connection weights, or training data. On the other hand, a black-box XAI method has no access to such information; it only knows about the input sample and the final output generated by the DL model. A big challenge of white-box methods is that we do not always have access to the model's internals. Moreover, only AI experts may be able to interpret those explanations derived from the model's internals. In applications where we are interested in understanding the behaviour of the AI model and discovering its vulnerabilities, e.g. in **software testing**, black-box explanations can be more helpful.

Various explanation methods have been developed for computer vision applications (Bach et al., 2015; Fong & Vedaldi, 2017; Montavon, Lapuschkin, Binder, Samek, & Müller, 2017; Nguyen, Dosovitskiy, Yosinski, Brox, & Clune, 2016; Zintgraf, Cohen, Adel, & Welling, 2017). However, most of these methods focus on white-box explanation, i.e. they need to have access to the ML model's internals. So far, few studies have addressed black-box explanation of DL models for image processing tasks. Randomized Input Sampling for Explanation (RISE) (Petsiuk, Das, & Saenko, 2018) estimates a saliency map through probing the object classification model using randomized masking of the input image. It estimates importance scores for pixels of the input image by computing the difference between class probabilities before and after masking the image. Detector Randomized Input Sampling for Explanation (D-RISE) (Petsiuk et al., 2021) adopts the image masking strategy introduced by RISE and provides an attribution method for explaining object detection models. However, a main challenge with RISE and D-RISE is that they need probability scores over classes and an objectness score for every bounding box to estimate the saliency map, hence, they may not be useful when the user only has access to bounding box coordinates detected by the model. Another challenge is equal importance assignment to both relevant and irrelevant pixels, which is caused by masks generated in a random manner. This may cause some pixels to be masked more often than other pixels, resulting in a saliency map in which some elements have higher values because they appeared in more masks. Moreover, a random mask may involve relevant and irrelevant pixels to a detected object. In this case, the same importance is assigned to both the relevant and irrelevant pixels, whereas only masking the relevant pixels has effect on the model's output.

In this paper, we address the above challenges by proposing a new explanation method named **Black-box Object Detection Explanation by Masking** (BODEM). This explanation method is model-agnostic; it can be used to generate explanations for every object detection

system regardless of the underlying ML model. Moreover, it does not need to have access to class probabilities or objectness scores. This property makes BODEM suitable for black-box explanation scenarios where we only have access to bounding boxes predicted by the detection model. Our explanation method consists of three main stages, i.e. mask generation, model inquiry, and saliency estimation. Local and distant masks are generated to estimate the effect of locally relevant and globally irrelevant pixels within the input image. A local mask refers to an area perturbed within the boundaries of an object, while a distant mask refers to perturbations applied to pixels outside an object. Model inquiry, the detection model is probed with the masked images to examine how its output is changed when some input information is missed. Finally, based on how the model’s output differs from the original output after masking the input, the explanation method computes a saliency map in which the importance of pixels is estimated for every object detected by the ML model. The saliency map is finally used to visualize a heatmap that shows the importance of areas within the image to particular predictions.

We conducted extensive experiments on three object detection tasks, i.e. user interface control detection, airplane detection, and vehicle detection, using three popular object detection DL models, i.e. YOLO, R-CNN, and SSD. The experimental results show that BODEM can be effectively used to produce explanations that reveal how important different parts of an image are to particular detections produced by an object detector. Investigating the explanations generated by BODEM, we show that the behaviour of the detection models can be explained, which can help users understand the behaviour of object detectors. Using the explanations generated by BODEM, we reveal some vulnerabilities of the object detectors for particular types of objects.

We also conducted data augmentation experiments where we show that the BODEM’s local masking technique can be effectively used to generate new training samples. Incorporating the new masked images into fine-tuning the object detection models, we improved the accuracy of the models, as well as their robustness to samples where some parts of objects are covered. This can help to understand and address the current challenges that object detection models have.

2. Model-agnostic explanation method

In this section, we give a detailed description of the BODEM explanation method. As already explained, BODEM consists of three main stages, i.e. 1) mask generation, 2) model inquiry, and 3) saliency estimation. **Figure 1** illustrates the overall architecture of the explanation method. In the next subsections, we describe these three phases in detail.

Problem formulation: Let I be an input image with the size of $w \times h$. Given an object detector f , and a bounding box $b=(x_1, y_1, x_2, y_2)$ detected by f , the goal is to generate a saliency map SM that can be used to visualize a heatmap to explain the detection. A heatmap is a version of the input image on which the importance of pixels is represented by different colors in a defined spectrum. The saliency map SM has a size of $w \times h$, containing values that represent the importance of pixels within I to the bounding box b predicted by f . Our explanation model solves this problem in a black-box manner; it does not need to have access to the architecture, loss function, gradients, weights, or output probabilities of f . Furthermore, it does not require class probabilities and objectness scores for every bounding box detected by f . The main idea of our explanation method is to mask different regions (i.e. a set of neighboring pixels) in I , give the masked images to f , and estimate the importance of regions by measuring how much the output of f changes.

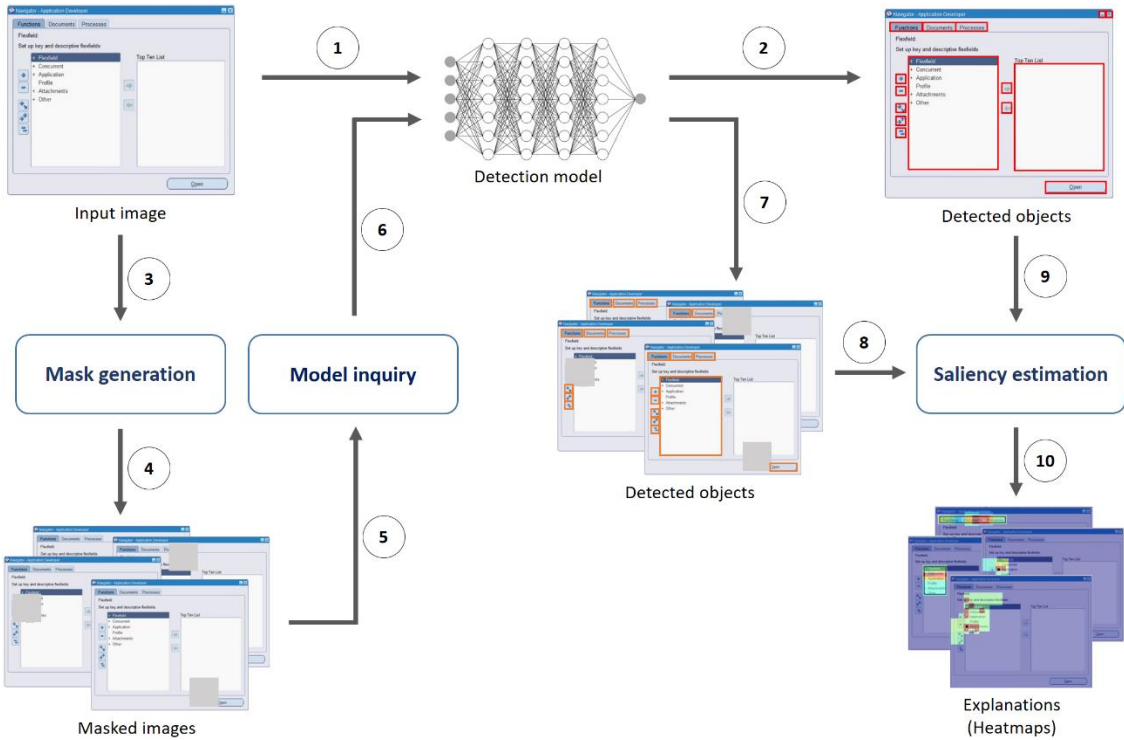


Figure 1. The overall architecture of BODEM explanation method. Final explanations are generated through several steps: 1) the input image is fed into the detection ML model, 2) the detection model predicts bounding boxes that specifies the detected objects, 3) the mask generation module receives the input image, 4) it then generates the masked images, 5) the model inquiry module receives the masked images, 6) it then passes the masked images to the detection model, 7) new predictions are generated for the masked images by the detection model, 8) new bounding boxes are given to the saliency estimation module, 9) the original bounding boxes detected by the ML models are also received by the saliency estimation module, and 10) the final explanations are generated as heatmaps through estimating the saliency of pixels.

2.1. Mask generation

As we already discussed in Section 1, a common strategy for black-box explanation of image processing models is to mask different parts of the input image and investigate how the model’s output changes when it is fed with the masked images. RISE (Petsiuk et al., 2018) and D-RISE (Petsiuk et al., 2021) adopted random masking strategies, however, random masking has its own challenges. First, all pixels in the input image may not have equal chance to be masked. Therefore, some pixels may be masked more often than the others. This can lead to explanations that do not represent the actual impact of pixels on a particular prediction. Second, relevant and irrelevant pixels to a particular prediction may be masked at the same time by a random mask. In this case, only the relevant pixels have effect on the model’s output, whereas the irrelevant pixels get importance scores as high as those of the relevant ones.

In order to address the above challenges, we propose two non-random masking strategies that help us identify local and global important pixels to a particular object detected by a ML model. We use local masks to investigate which parts of the detected object and which neighboring pixels have any impacts on the model’s output. We also use global masks to discover if the detection model predicts a bounding box with respect to other (and maybe irrelevant) parts of the input image.

2.1.1. Local masks

Given an input image I , and a bounding box $b=(x_1, y_1, x_2, y_2)$ detected by f , a set of local masks $LM=\{lm_1, lm_2, \dots, lm_N\}$ is generated by masking different parts of b and its neighboring pixels. A local masking area $MA=(x_1-5, y_1-5, x_2+5, y_2+5)$ is specified by considering the coordinates of b and five pixels around it. The masking procedure starts by dividing MA by two, separately in horizontal and vertical directions. The sub-areas are then recursively divided by two, again in horizontal and vertical directions, in order to have smaller sub-areas. This procedure continues until the size of a dimension of the smallest sub-area is smaller than 20 pixels. Every sub-area is masked by replacing the pixel values with the average of pixel values within the sub-area.

Figure 2 shows an example where the underlying task is to detect user interface controls within screenshots taken from software windows. In this figure, a bounding box detected by the object detection model is represented by the orange rectangle, and the local masking area specified by the explanation method is represented by the green rectangle. **Figure 3** shows 44 local masks generated by our explanation method for the object detected in **Figure 2**. For brevity reasons,

only the masking area is shown in this example. However, in the mask generation step, every mask is generated for a copy of the whole input image.

Algorithm 1 gives the pseudo code of the procedure for generating local masks. First, an empty set of locally masked images is initialized (line 3). A local masking area is specified with respect to the bounding box's coordinates, and an empty set of sub-areas SA is initialized (lines 4-5). Then, if the height and weight of the masking area are not smaller than 20 pixels, the masking area is horizontally and vertically divided by two, and the resulting sub-areas are added to SA (lines 6-9). Every sub-area in SA is repeatedly divided horizontally and vertically by two, and new sub-areas are created, until the height or width becomes smaller than 20 pixels (lines 10-17). Finally, for every sub-area created in the previous steps, a masked copy of the original input image is generated with respect to the coordinates of the sub-area (lines 18-23).

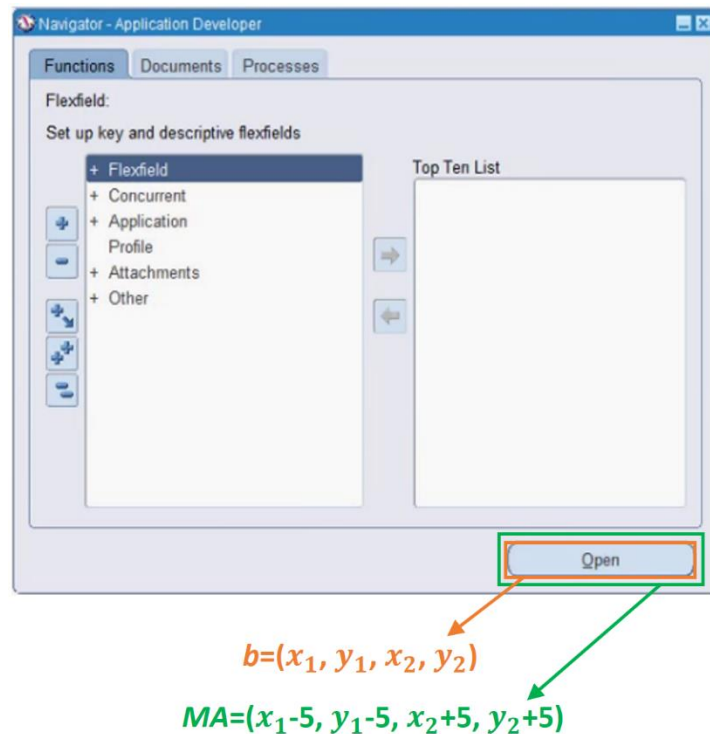


Figure 2. A bounding box b detected by a detection model f , and a masking area MA specified by our explanation method to generate local masks for b . In this example, the underlying task is to detect user interface controls within screenshots taken from software windows.



Figure 3. Forty four local masks generated by our explanation method for the object detected in Figure 2. For brevity reasons, only the masking area is shown in this example. However, in the mask generation step, every mask is generated for a copy of the whole input image.

2.1.2. Global masks

While local masks are used to estimate the importance of pixels within a detected object and its neighborhood, we use global masks to investigate if other parts of the input image, which may be irrelevant to the detected object, have any effects on the object detection model’s output. Global masks are generated in two sizes, i.e. 20×20 and 50×50 pixels. We selected these two sizes heuristically with respect to the visual quality of heatmaps and the size of input images we used in our experiments. Masking squares larger than 50×50 would lead to an inaccurate saliency map where many pixels get the same important score because they belong to a large mask, while their actual effects on the model’s output may be different. On the other hand, very small masked sub-areas (e.g. smaller than 20×20) may convey no or little information, hence, they may have no or little effect on the model’s output, whereas our goal is to understand if the object detection model uses information available in other areas within the image to make local decisions.

The procedure of producing global masks starts with masking a square with the specified size (e.g. 20×20 or 50×50) at the uppermost-leftmost part of the image. Then, the mask area, i.e. the square, moves separately in horizontal and vertical directions, and new masked images are produced until we reach the lowermost-rightmost part of the image. Every pixel within the input image exactly appears once in a global mask. Similar to local masks, as explained in **Section 2.1.1**, pixel values in a global mask are replaced with the average value of the pixels within the respective global mask area.

Figure 4 shows a schematic representation of the grid that refers to how global masks are generated by the explanation method for an input image. In the global masking procedure, every

square (or rectangle) within the image is masked only once. In each masked copy of the input image, only one square (or rectangle) is masked. The size of squares in global masks is customizable and can be modified depending on the task at hand and the size of input image.

Algorithm 1. The local masking procedure used by the BODEM explanation method.

```

1: Input: input image  $I$ , bounding box  $d=(x_1, y_1, x_2, y_2)$  detected by  $f$ 
2: Output: a set of locally masked images  $LM$ 
3:  $LM=\emptyset$ 
4: specify a local masking area:  $MA=(x_1-5, y_1-5, x_2+5, y_2+5)$ 
5: create a set of sub-areas  $SA=\emptyset$ 
6: if the height of  $MA$  is not smaller than 20 pixels:
7:   then divide  $MA$  horizontally by two and add the resulting sub-areas to  $SA$ 
8: if the width of  $MA$  is not smaller than 20 pixels:
9:   then divide  $MA$  vertically by two and add the resulting sub-areas to  $SA$ 
10: while a unique sub-area is added to  $SA$ , repeat steps 11 to 16:
11:   for every sub-area  $sa_i$  in  $SA$ :
12:     if the height of  $sa_i$  is not smaller than 20 pixels:
13:       then divide  $sa_i$  horizontally by two and add the resulting sub-areas to  $SA$ 
14:     if the width of  $sa_i$  is not smaller than 20 pixels:
15:       then divide  $sa_i$  vertically by two and add the resulting sub-areas to  $SA$ 
16:   end for
17: end while
18: for every sub-area  $sa_i$  in  $SA$ :
19:   specify mask coordinates:  $X_1=sa_i["x_1"]$ ,  $Y_1=sa_i["y_1"]$ ,  $X_2=sa_i["x_2"]$ ,  $Y_2=sa_i["y_2"]$ 
20:   create a copy of input image:  $I'=I$ 
21:    $I'[X_1:X_2, Y_1:Y_2] = \text{Mean}(I'[X_1:X_2, Y_1:Y_2])$ 
22:   add  $I'$  to the set of locally masked images  $LM$ 
23: end for
24: return  $LM$ 

```

2.2. Model inquiry

The model inquiry module acts as an intermediary between the explanation model and the object detection model. It receives locally and globally masked images, sends them to the object detection model, receives new bounding boxes detected by the object detector, and passes them

to the next step, i.e. the saliency estimation module. The inquiry module is model-agnostic and has no information about the neural network architecture, loss function, activation functions, connection weights, and hyperparameters of the underlying ML model. It sends queries to the detection model and receives bounding box coordinates predicted by the model. Therefore, the explanation method can be used to explain any object detection systems, regardless of the underlying ML model, making it suitable for black-box software testing scenarios.

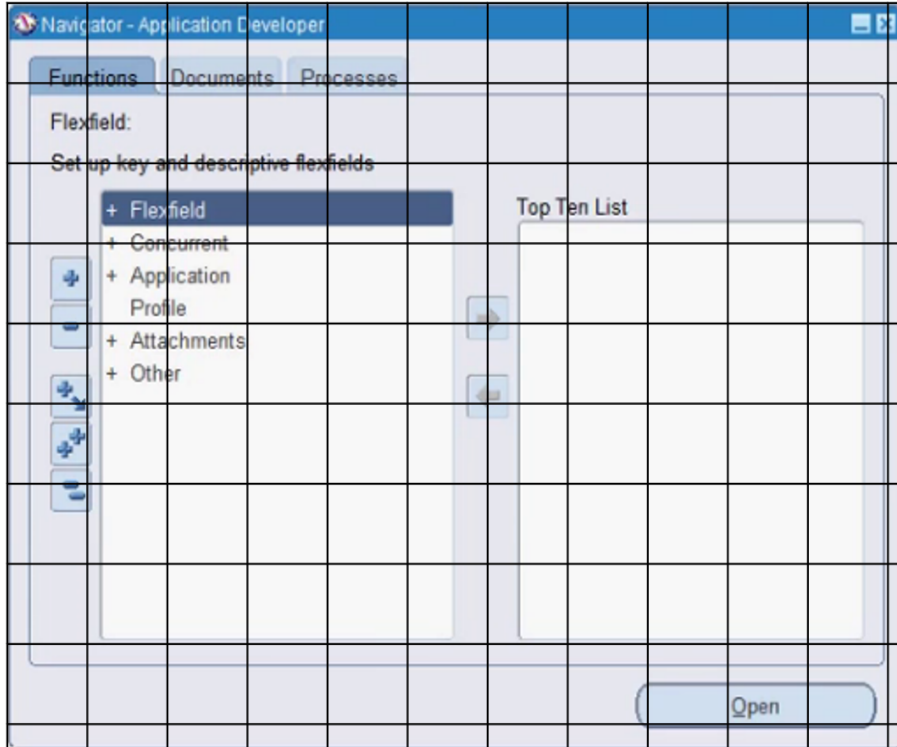


Figure 4. Schematic representation of the grid that refers to how global masks are generated by the explanation method for an input image. In the global masking procedure, every square (or rectangle) within the image is masked only once. Only one square (or rectangle) is masked within a masked copy of the input image.

2.3. Saliency estimation

The saliency estimation module receives the original prediction produced by the object detection model and new predictions produced for local and global masks. Its main task is to estimate the importance of pixels within the input image by measuring the difference between the original and new predictions. It then generates a heatmap that visualizes the importance of different parts of the input image for a particular object detected by the ML model.

Given an input image I with the size of $w \times h$, an original bounding box $b = (x_1, y_1, x_2, y_2)$ detected by f , a set of local masks $LM = \{lm_1, lm_2, \dots, lm_N\}$, a set of global masks $GM = \{gm_1, gm_2, \dots, gm_J\}$, and a set of new bounding boxes $B' = \{b'_1, b'_2, \dots, b'_K\}$ detected by f for every locally or

globally masked copy of I , where $b'_k = (x'_1, y'_1, x'_2, y'_2)$, the goal is to compute a saliency map SM that is a matrix with the size of $w \times h$. This saliency map estimates the importance of pixels within I .

First, for every $lm_n \in LM$, the similarity between the original bounding box and the new bounding boxes is measured as the maximum Intersection Over Union (IOU) between b and every $b'_k \in B'$, as follows:

$$Similarity(b, B') = \max_{b'_k \in B'} IOU(b, b'_k) \quad (1)$$

If the similarity, which is a value in the range $[0, 1]$, is larger than a threshold *IOU-threshold*, it means an object has been detected within the masked image that has a considerable amount of shared area with the object detected within the original image. In this case, the original detected bounding box b is similar enough to a detected bounding box $b'_k \in B'$ in the masked image, therefore, the difference between b and B' is estimated as zero. The goal of using *IOU-threshold* is to specify how much dissimilarity between the original and new detections is tolerated by the explanation method.

On the other hand, if the similarity is smaller than *IOU-threshold*, there is a considerable difference between the original bounding box b and the new bounding boxes B' detected within the masked image. In this case, the difference between b and B' is estimated by measuring the minimum distance between b and every $b'_k \in B'$, as follows:

$$Difference(b, B') = \min_{b'_k \in B'} Distance(b, b'_k) \quad (2)$$

where the distance between a pair of bounding boxes is defined as the inverse of IOU between the boxes, as follows:

$$Distance(b, b') = \frac{1}{IOU(b, b')} \quad (3)$$

In this way, the larger the IOU between the original and new bounding boxes, the smaller the difference between b and B' , and vice versa.

Now that the difference between b and B' has been measured, the saliency map SM is updated to estimate the importance of pixels that are masked within the local mask lm_n . The saliency map is updated by adding the difference between b and B' to the current value of those elements in SM that represents the pixels masked within the local mask lm_n , as follows:

$$SM[lm_n] = SM[lm_n] + Difference(b, B') \quad (4)$$

Finally, if no new object is detected by the detection model in the masked image, it means pixels within lm_n have a large impact on the model's output, such that the model has not been able

to detect any objects. In this case, a large value must be added to the respective values within SM to reflect the impact of the maxed pixels. We heuristically selected $w+h$ as the large value with respect to the visual quality of the heatmap that is generated using the saliency map.

The same saliency estimation process performed for local masks is also performed for every global mask $gm_j \in GM$, and SM is updated in the same way described for local masks.

After finishing the saliency estimation step, for those local or global masks that caused no difference between the original and new bounding boxes, SM is equal to zero as the estimated importance. For those masks that caused small changes in the model's output, SM has small values as the estimated importance. For masks that led to large changes in the output of the detection model, SM contains large values as the estimated importance.

Algorithm 2. The saliency estimation procedure used by the BODEM explanation method.

```

1: Input: input image  $I$ , bounding box  $d=(x_1, y_1, x_2, y_2)$  detected by  $f$ , set of local masks
 $LM=\{lm_1, lm_2, \dots, lm_N\}$ , set of global masks  $GM=\{gm_1, gm_2, \dots, gm_J\}$ , set of new bounding
boxes  $B'=\{b'_1, b'_2, \dots, b'_K\}$  detect for every locally or globally masked image
2: Output: saliency map  $SM$ 
3:  $SM[0:w, 0:h]=0$ 
4: for every local mask  $lm_n \in LM$ :
5:   measure the similarity between  $b$  and  $B'$  using Equation (1)
6:   if  $Similarity(b, B')$  is larger than  $IOU$ -threshold:
7:     then  $Difference(b, B')=0$ 
8:     if  $Similarity(b, B')$  is smaller than  $IOU$ -threshold:
9:       then measure  $Difference(b, B')$  using Equations (2) and (3)
10:      update  $SM[lm_n]$  using Equation (4)
11:      if no objects have been detected when  $I$  was masked by  $lm_n$ :
12:        then  $SM[lm_n] = SM[lm_n]+w+h$ 
13: end for
14: for every global mask  $gm_j \in GM$ :
15:   repeat steps 5 to 12
16: end for
17: return  $SM$ 

```

Values in the saliency map SM are then normalized to be in the range $[0, 1]$. In the last stage of the explanation method, a heatmap is visualized by mapping SM on the input image. The

heatmap shows different values within SM with different colors, indicating different levels of importance.

Algorithm 2 gives the pseudo code of the procedure for saliency estimation. First, the saliency map is initialized with the size of $w \times h$, and all the elements are set to zero (line 3). Then for every local mask, the similarity between the original and new bounding boxes is measured, and the difference between bounding boxes is used to update the saliency maps for those pixels that belong to the respective mask (lines 4-13). The same processes are also done for every global mask (lines 14-16). Finally, the saliency map is used to visualize a heatmap that shows which parts of the input has more impact on generating a particular prediction by the object detection model. **Figure 5** shows a heatmap generated by the BODEM explanation method for an object detected by YOLO. The task is to detect user interface controls within screenshots taken from software windows. In this example, the value of $IOU\text{-}threshold$ is set to 0.8. The target object is indicated by the black rectangle. As the heatmap shows, masking different parts of the target object had different levels of impact on the accuracy of the ML model. Moreover, only the pixels within the local masking area of the target object had effect on detecting the user interface control. **Figure 6** shows the masks for which the object detection model could not detect the correct bounding box. For each pair of bounding boxes, the black rectangle shows the target bounding box, and the red rectangle indicates the new bounding box detected for the masked image. The IOU values are also presented for each pair. These new bounding boxes led to generating the heatmap shown in **Figure 5**. In this example, only the new bounding boxes whose IOU with the target bounding box was smaller than $IOU\text{-}threshold=0.8$ were used to update the saliency map.

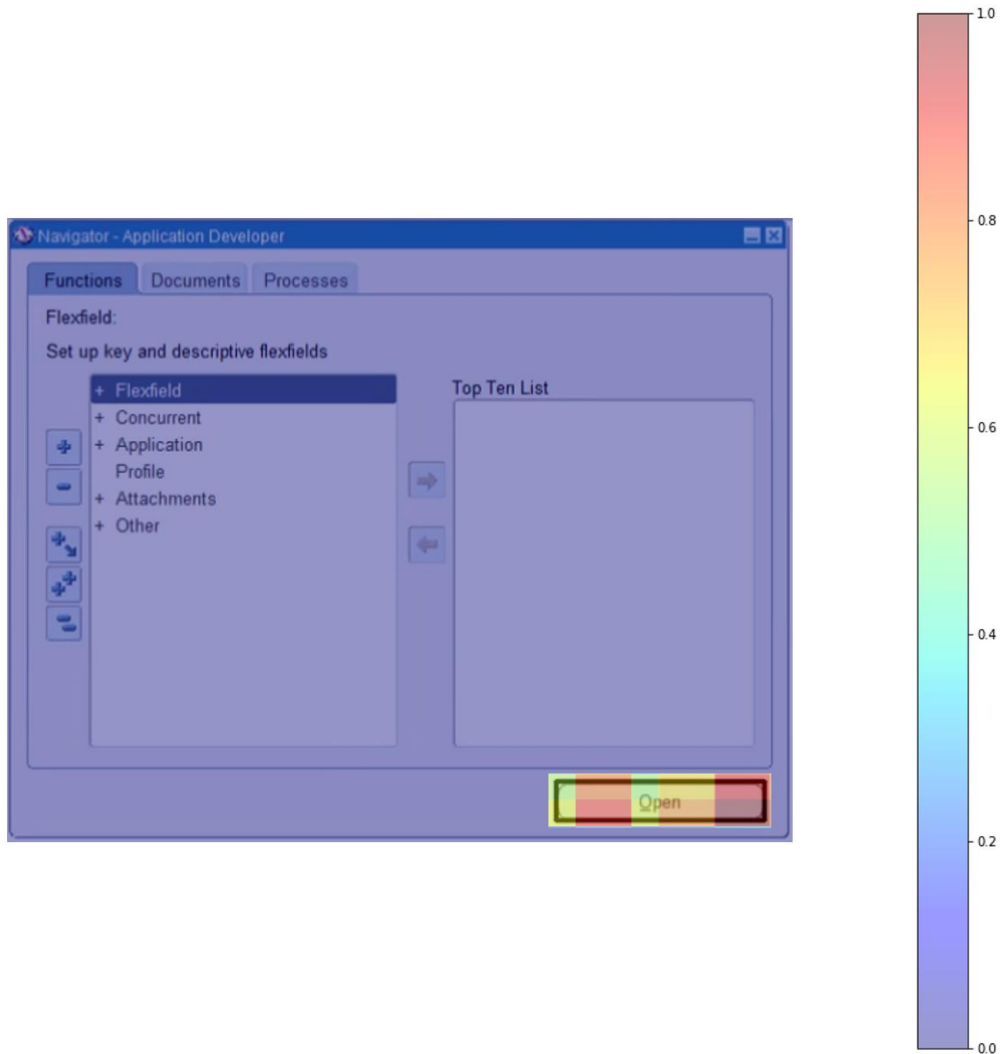


Figure 5. A heatmap generated by the BODEM explanation method for an object detected by YOLO. The task is to detect user interface controls within screenshots taken from software windows. The target object is indicated by the black rectangle. As the heatmap shows, masking different parts of the target object had different levels of impact on the accuracy of the ML model.

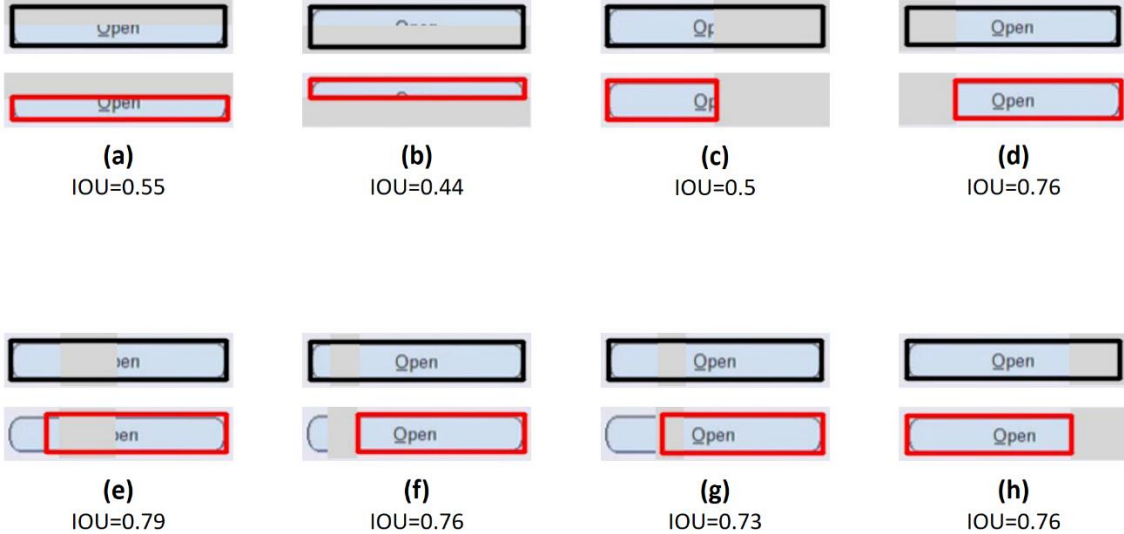


Figure 6. Masks for which the object detection model could not detect the correct bounding box. For each pair of bounding boxes, the black rectangle shows the target bounding box, and the red rectangle shows the new bounding box detected for the masked image. These new bounding boxes led to generating the heatmap shown in Figure 5.

3. Experimental results

In this section, we first describe the datasets and object detection models that we utilized in our experiments. We then presents the object detection test results, as well as explanations produced by our BODEM explanator. Moreover, we give examples where explanations can help to analyze which parts of objects are more important to the object detectors. We finally present and discuss data augmentation experiments where we used local masks to improve the accuracy of the object detectors and help them decrease their error rate on detecting specific objects.

3.1. Datasets

User interface control detection: Our main focus for developing the explanation method was on the user interface control detection task for automated software testing. This is a private dataset, which contains 16,155 images annotated for detection and classification of 18 types of user interface controls. The images are digital screenshots taken from desktop, Software as a Service (SaaS), and mobile applications. We split the dataset into a train and development set containing 14,155 images, and a test set containing 2,000 images.

Airplane detection: This public dataset contains 733 aerial images annotated for detecting airplanes. We split the dataset into a train and development set with 650 images, and a test set with 83 images. We chose to use this small dataset in order to investigate how the BODEM

explanation method can be effective in scenarios where there are not many images to train an object detection model.

Vehicle detection: Common Objects in Context (COCO) dataset (Lin et al., 2014) is a large dataset of more than 160,000 images annotated for object detection and classification of 80 object categories. We created a subset of 8,000 images from COCO for our vehicle detection task by randomly choosing 2,000 images from each one of the categories “CAR”, “BUS”, “TRUCK”, and “MOTORCYCLE”. The train and development set of this new dataset has 7,000 images. The test set contains 1,000 images.

3.2. Object detection models

Object detection models can be generally divided into one-stage and two-stage methods. Two-stage detectors break down the problem into two steps, i.e. 1) detecting region proposals, which possibly contain an instance of an object of interest, and 2) classifying those regions with respect to the probability of an object appearing within a region. On the other hand, one-stage detectors utilize end-to-end neural networks to predict bounding boxes and class probabilities of detected objects all at once. We used both one-stage and two-stage object detection models in our experiments.

YOLO (Redmon et al., 2016): It is a one-stage object detection algorithm that divides the input image into N grids with equal size, and then detects and localizes objects within each grid. In order to handle overlapping bounding boxes detected within different grids, YOLO utilizes Non-Maximal Suppression (NMS), which is a technique to filter grids and select regions with the highest probability of containing an object of interest. Due to its one-stage detection strategy, YOLO can perform much faster than popular two-stage detectors such as R-CNN and Fast R-CNN. That is why it is widely used for real-time object detection. Inspired by the GoogleNet architecture, YOLO composes of 24 convolutional layers followed by two fully-connected layers. We used YOLO-v5 in our experiments, and trained it on the user interface control detection dataset.

R-CNN (Girshick et al., 2014): This object detector uses selective search to extract region proposals, which are then fed to a CNN that classifies the regions as they contain a target object or not. As the backbone of this object detector, we used a VGG-16 model, which has a CNN with 16 convolutional layers and 134 million parameters. This CNN was already pretrained on more than one million images from the ImageNet dataset¹. One flatten layer, two fully-connected dense

¹ <https://www.image-net.org/>

layers, and a softmax layer for the final classification were added to the backbone model. We freezed all layers of the backbone except the last three convolutional layers. We then fine-tuned the remaining layers and our custom layers on the airplane detection dataset.

SSD (Wei Liu et al., 2016): It is another one-stage detection model that is composed of two components, i.e. a backbone model, and SSD head. A pretrained model is usually utilized as the backbone to serve as a feature extractor. SSD head is usually formed by several convolutional layers on top of the backbone. These additional layers are specifically trained for the object detection task at hand. In our experiments, we used a variant of SSD that has ResNet-101, which were pretrained on ImageNet, with around 44 million parameters as the backbone. Six more convolutional layers were added on top of the backbone to form the SSD head and train it for our object detection task. We fine-tuned the SSD model on the vehicle detection dataset.

3.3. User interface control detection

We trained the YOLO detection model on the user interface control detection dataset. **Table 1** presents the performance scores obtained by the YOLO object detection model on the respective test set. **Figure 7** shows an image from the user interface control detection dataset, the bounding boxes that show the objects detected by the YOLO detection model, and the heatmap generated by the BODEM explanation method. In this example, the detection model could not detect four input controls. As can be seen in this explanation, masking different areas has different amounts of effect on the accuracy of the object detector. As already expected, masking user interface controls has higher effects than masking those areas where no user interface controls exist. However, there are controls for which the YOLO object detector was still able to detect the correct boundaries, regarding an IOU-threshold of 0.8, although some parts of the controls were masked.

In order to have explanations even for those controls for which the object detector was able to detect the correct boundaries regarding the IOU-threshold of 0.8, we utilized a dynamic threshold approach such that the IOU-threshold gradually increased by 0.05 until the IOU between the original and new bounding boxes falls below the threshold. If the IOU-threshold reaches 1.0 and no incorrect boundary boxes are produced by the object detector, masking has no effect on the object detector’s performance, therefore, no important areas are shown on the heatmap for that control.

Figure 8 shows explanations produced for five controls from **Figure 7**. These explanations were generated using the dynamic threshold approach, therefore, they may be different from the explanation shown in **Figure 7**. For clarity reasons, the boundary box predicted by the object detector is also represented for the target control in each explanation. As can be seen, not every

part of the objects has equal importance to predicting the correct boundary boxes. In the explanations (a) and (b), it can be seen that those areas that contain text around the target control have more effect on the prediction. The explanations (c) and (d) suggest that for those BUTTON controls that contain an icon, the correct prediction of bounding box is to a high extent dependent to the icon. The explanation (e) shows that for the relatively large DROPDOWN control, masking only few parts of the control can mislead the object detector. In this way, we may infer that most parts of this control are equally important to predicting the bounding box. We observed similar explanations for several images in the user interface control detection dataset.

Table 1. Performance scores obtained by the YOLO object detection model on the user interface control detection test set.

Class	Precision	Recall	mAP@.5	mAP@.95
ALL	0.799	0.752	0.75	0.588
ICON	0.931	0.88	0.883	0.611
DROPDOWN	0.886	0.907	0.904	0.748
BUTTON	0.893	0.861	0.886	0.773
MENU	0.836	0.512	0.523	0.4
INPUT	0.913	0.748	0.758	0.663
LIST	0.674	0.709	0.636	0.481
TABBAR	0.905	0.582	0.645	0.562
TABLE	0.815	0.862	0.825	0.747
RADIO_SELECTED	0.916	0.916	0.946	0.68
RADIO_UNSELECTED	0.856	0.957	0.918	0.688
CHECKBOX_UNCHECKED	0.891	0.94	0.925	0.654
CHECKBOX_CHECKED	0.905	0.887	0.904	0.591
TREE	0.77	0.769	0.749	0.63

Observing many explanations produced by the YOLO object detector helped us find some patterns that can be useful for inspection and validation of the detection model: 1) lines that specify the borders of controls are very important to the model, 2) icons within BUTTON controls have high impacts on detecting correct boundaries, 3) correct detection of small controls, such as CHECKBOX, is highly dependent on the neighboring areas within the image, such that perturbing small parts of neighboring area can mislead the object detector, 4) texts within controls such as MENU have large effects on the correct predictions, 5) detecting those BUTTON controls that are close to other controls is also influenced by the borders of neighboring controls, in addition to

the control's borders, and other similar patterns. These observations convey that explanations generated by BODEM can effectively help to understand the behavior of the detection model.

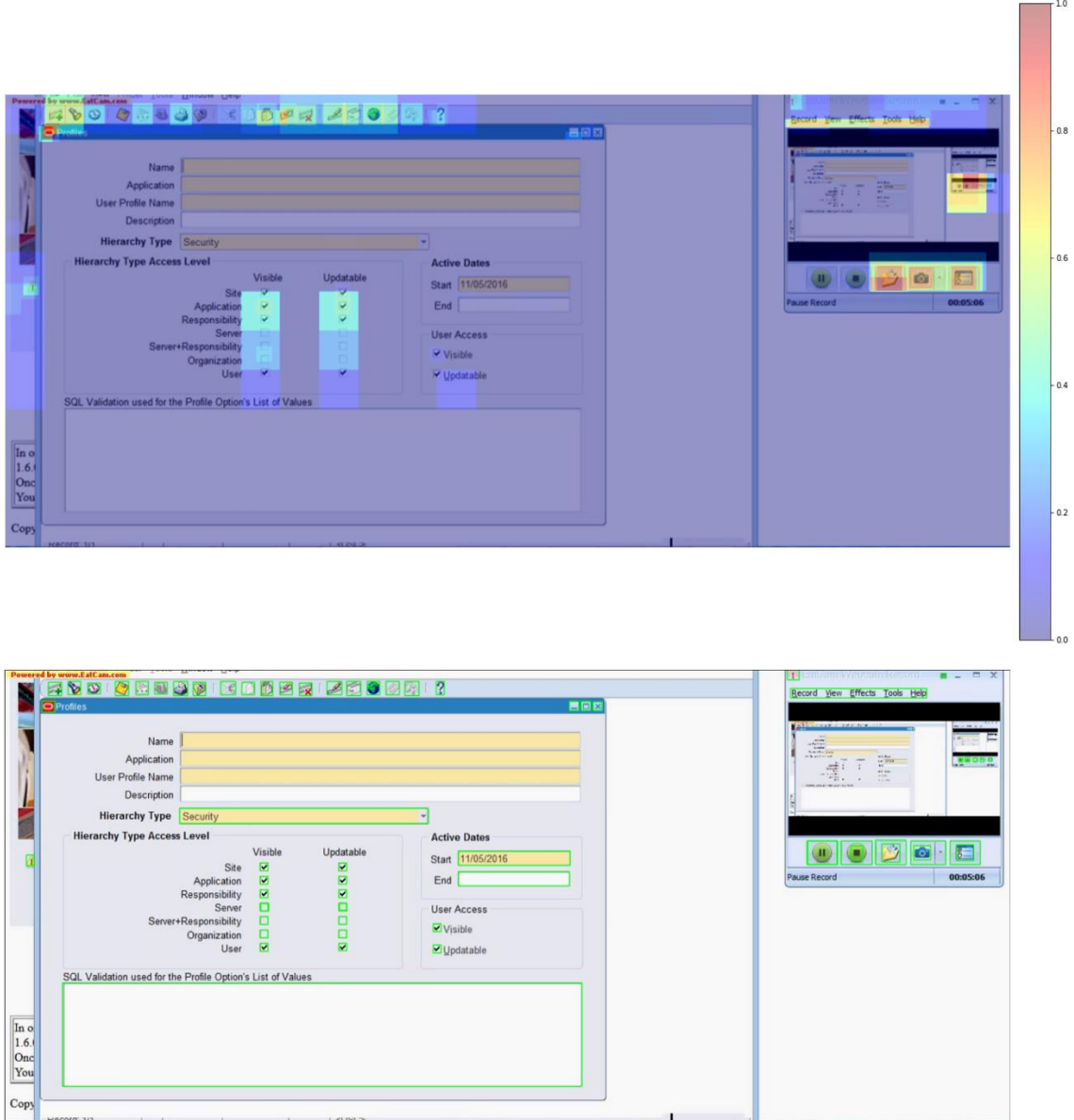


Figure 7. An image from the user interface control detection dataset, the bounding boxes that show the objects detected by the YOLO detection model, and the heatmap generated by the BODEM explanation method. In this example, the detection model could not detect four input controls. As can be seen, no important areas are identified for some controls regarding the IOU-threshold of 0.8. Using a smart threshold approach, we generated explanations even for these specific controls, which are shown in Figure 8.

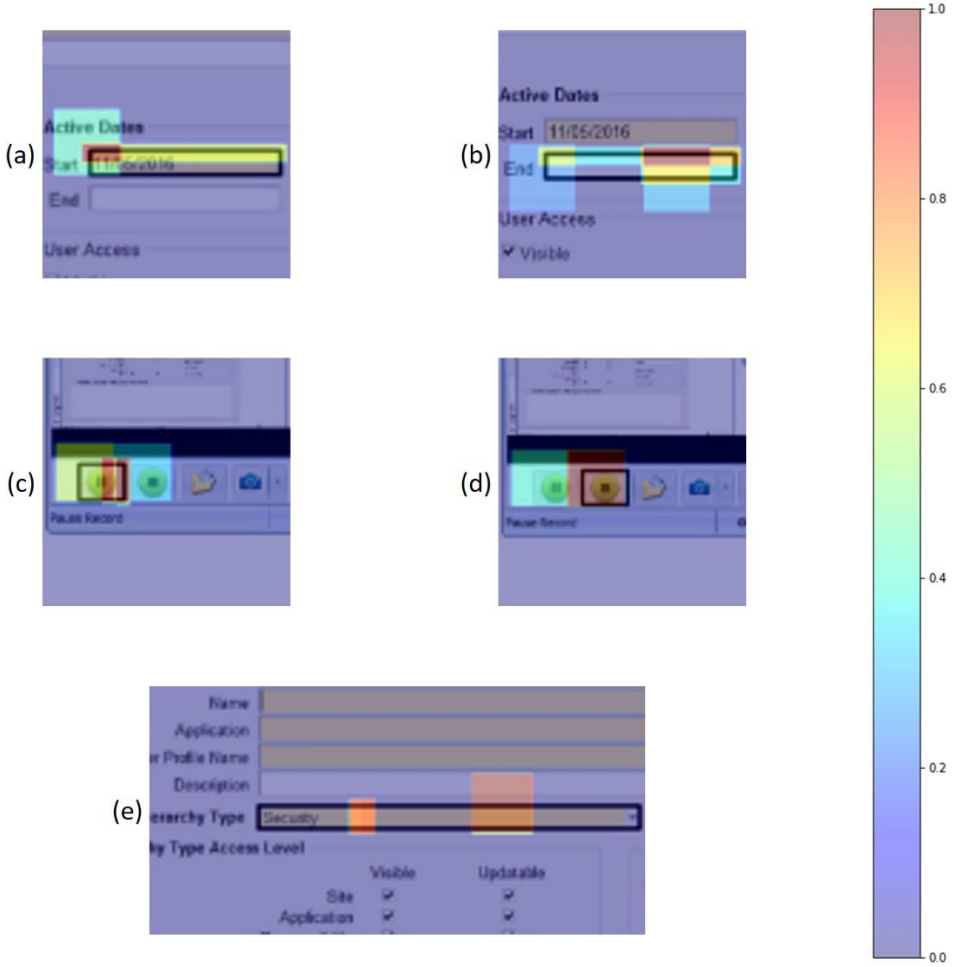


Figure 8. Explanations produced for five controls from Figure 7. These explanations were generated using the dynamic threshold approach, therefore, they may be different from the explanation shown in Figure 7. For clarity reasons, the boundary box predicted by the object detector is also represented for the target control in each explanation.

3.4. Airplane detection

We trained the R-CNN detection model on the airplane detection dataset. The model achieved an accuracy of 87.05% on the test set. We utilized our BODEM explanation method to understand which parts of the objects detected by the detection model are more important and have higher impacts on the model’s decisions. **Figure 9** shows two images from the airplane detection dataset, the bounding boxes that show the objects detected by the R-CNN detection model, and the heatmaps generated by the BODEM explanation method. As the explanations show, the head, wings and tail of the airplanes have more impact than other parts on detecting the airplanes. This is a common pattern in many objects detected by the model, suggesting that the object detector decides about the bounding boxes by paying more attention to the head, wings, and head of an airplane.

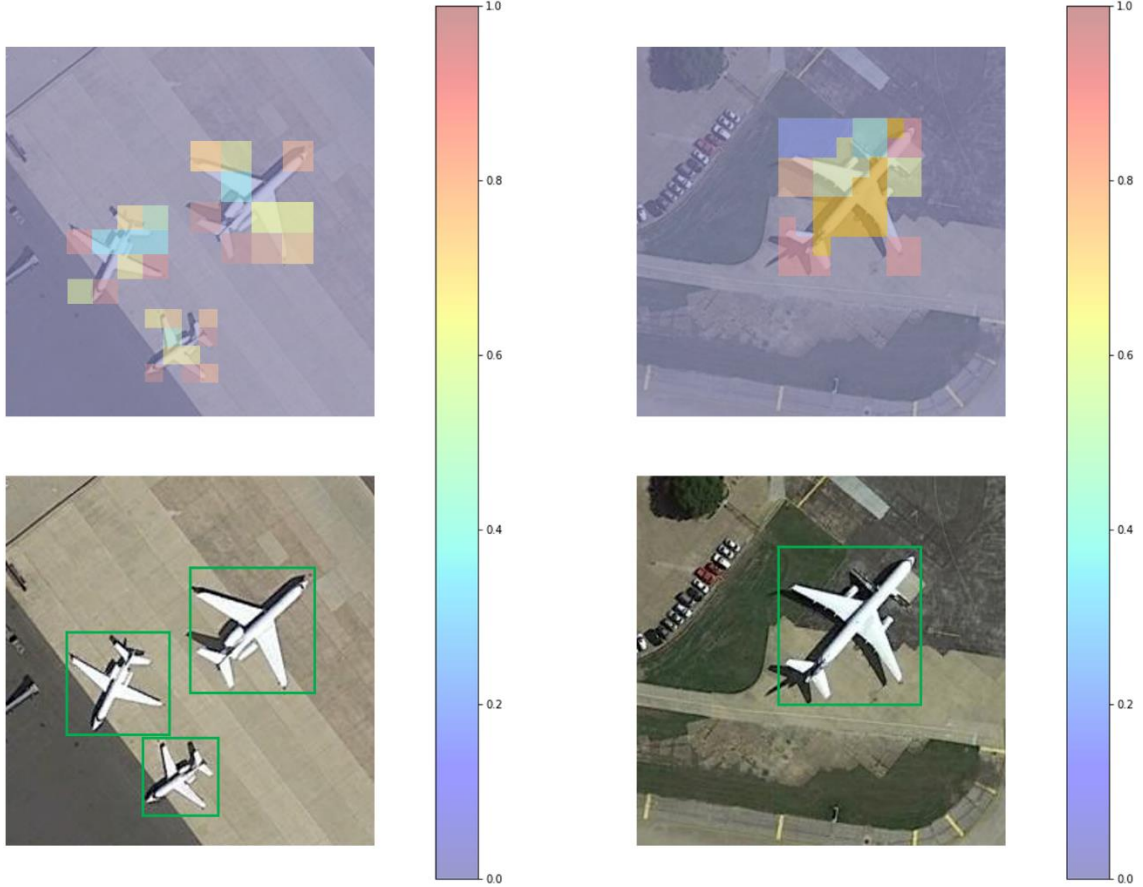


Figure 9. Two images from the airplane detection dataset, the bounding boxes that show the objects detected by the R-CNN detection model, and the heatmaps generated by the BODEM explanation method.

3.5. Vehicle detection

We trained the SSD detection model on the vehicle detection dataset. **Table 2** presents the performance scores obtained by the SSD object detection model on the respective test set. **Figure 10** shows two images from the vehicle detection dataset, the bounding boxes that show the objects detected by the SSD detection model, and the heatmaps generated by the BODEM explanation method. Car, truck, bus, and motorcycle are shown by green, purple, orange, and yellow bounding boxes, respectively. As the explanations show, the head, wheels, and lower parts of the truck had a higher importance to the detection model. The wheels, hood, and boot had higher impacts on detecting the car. The wheels and seat were more important for detecting the motorcycle. The object detector paid more attention to the head and wheels of the bus for predicting the bounding box. Observing several explanations, we found similar patterns in the objects detected by the SSD detection model on the vehicle detection dataset.

Table 2. The performance scores obtained by the SSD detection model on the vehicle detection test set.

Class	Precision	Recall	mAP@.7
ALL	0.813	0.780	0.765
CAR	0.844	0.801	0.783
BUS	0.819	0.781	0.765
TRUCK	0.785	0.752	0.742
MOTORCYCLE	0.803	0.788	0.771

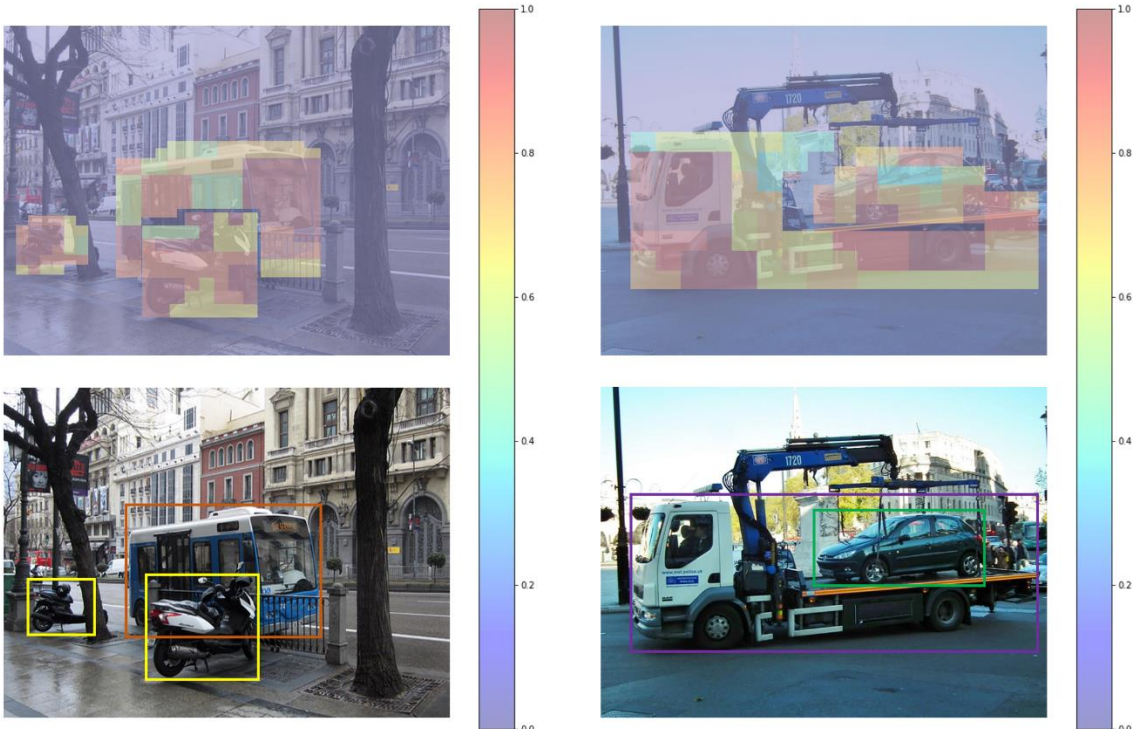


Figure 10. Two images from the vehicle detection dataset, the bounding boxes that show the objects detected by the SSD detection model, and the heatmaps generated by the BODEM explanation method. Car, truck, bus, and motorcycle are shown by green, purple, orange, and yellow bounding boxes, respectively.

3.6. Data augmentation

Data augmentation can be regarded as a regularization technique to improve the generalization performance of ML systems (Moradi & Samwald, 2022b). In data augmentation, some modifications are applied to original training samples, and different modified versions are used for further training or fine-tuning the target ML model. We conducted a set of data augmentation experiments by using the local masking technique, which we introduced as a part of the BODEM explanation method, in order to investigate how the object detection performance

can be improved by fine-tuning the object detectors on masked images. However, we performed the masking and data augmentation procedures in a way that the weaknesses of the object detectors can be addressed.

3.6.1. User interface control detection

Investigating those samples for which the YOLO object detector could not correctly predict bounding boxes, we found that detecting large controls such as TABLE, MENU, LIST, and TABBAR is more challenging than smaller controls. Especially when some parts of these large controls are masked by other controls, the detection model has problems with predicting the correct boundaries. Moreover, these controls often contain other lines than just their borders, hence, it is more challenging for the object detector to detect the correct borders. In software test automation, table detection is one of the big challenges. Quite often tables (or other large controls) do not fit inside the user screen or are covered by other objects appearing in the screen. Therefore, object detection models have difficulties detecting tables or any relatively large user interface controls. In order to address the above-mentioned challenges, we used the local masks produced by BODEM to generate perturbed samples for data augmentation.

We randomly selected 6,000 images from the training set of the user interface control detection dataset and produced at least 20 different versions of each image by applying the local mask generation method described in **Section 2.1.1**. The local masks were only produced for TABLE, MENU, LIST, and TABBAR controls, such that each perturbed version of an image contained only one mask for one of the four controls. The number of masked images per control was proportional to the number of target controls within the image. For example, for images that contained 2, 4, and 5 instances from the four aforementioned controls, the number of different masked versions of the image per control was 10, 5, and 4, respectively. We rounded up this number in case the number of masked images per control was not an integer. We then created a new training set by combining the original training samples and the masked images, and fine-tuned the YOLO model on the new training set. We also created a new test set by randomly selecting 200 images from the original test set and applying the local masking method to generate at least 10 different masked versions for each image. The number of masked versions of an image per control was specified in the same way we described for the new training set.

Table 3 presents the performance scores obtained by the original and fine-tuned YOLO detection models for all the control types. The results are given on the original and masked test samples. The average scores on both the original and masked test sets are presented as well. As the results show, the original model slightly performed better than the fine-tuned model on the original test set. However, the fine-tuned object detector performed much more accurately than

the original model on the masked test samples. The fine-tuned model also performed considerably better than the original model regarding the average of scores on both the original and masked test sets.

Table 3. Performance scores obtained by the original and fine-tuned YOLO object detectors on the original and masked test samples for **ALL** controls. The average of performance scores on the original and masked test sets is reported as well. The best score between the original and fine-tuned models is shown in underlined face separately for original, masked, and average test results.

Test set	Detection model	Precision	Recall	mAP@.5	mAP@.95
Original test set	Original	<u>0.799</u>	<u>0.752</u>	<u>0.750</u>	<u>0.588</u>
	Fine-tuned	0.793	0.750	0.742	0.583
Masked test set	Original	0.757	0.713	0.688	0.524
	Fine-tuned	<u>0.811</u>	<u>0.759</u>	<u>0.764</u>	<u>0.608</u>
Average	Original	0.778	0.732	0.719	0.556
	Fine-tuned	<u>0.802</u>	<u>0.754</u>	<u>0.753</u>	<u>0.595</u>

Table 4. Performance scores obtained by the original and fine-tuned YOLO object detectors on the original and masked test samples for **TABLE** control. The average of performance scores on the original and masked test sets is reported as well. The best score between the original and fine-tuned models is shown in underlined face separately for original, masked, and average test results.

Test set	Detection model	Precision	Recall	mAP@.5	mAP@.95
Original test set	Original	0.815	<u>0.862</u>	<u>0.825</u>	<u>0.747</u>
	Fine-tuned	<u>0.840</u>	0.833	0.814	0.731
Masked test set	Original	0.816	0.660	0.516	0.418
	Fine-tuned	<u>0.822</u>	<u>0.827</u>	<u>0.777</u>	<u>0.701</u>
Average	Original	0.815	0.761	0.670	0.582
	Fine-tuned	<u>0.831</u>	<u>0.830</u>	<u>0.795</u>	<u>0.716</u>

The performance scores obtained by the original and fine-tuned YOLO models for TABLE, MENU, LIST, and TABBAR controls are presented in **Table 4**, **Table 5**, **Table 6**, and **Table 7**, respectively. The average scores on both the original and masked test sets are presented as well. As the results show, the original model can again perform better than the fine-tuned model on the original samples for all the four controls. However, the fine-tuned model achieved the highest scores on the masked test images for three controls, i.e. TABLE, LIST, and TABBAR. Regarding the average of scores on both the original and masked test samples, the fine-tuned detection model again performed more accurately than the original model for those three controls. The fine-tuned

model, however, was not able to achieve higher scores than the original model for MENU control, with respect to the average results and the scores on the masked test set.

Table 5. Performance scores obtained by the original and fine-tuned YOLO object detectors on the original and masked test samples for **MENU** control. The average of performance scores on the original and masked test sets is reported as well. The best score between the original and fine-tuned models is shown in underlined face separately for original, masked, and average test results.

Test set	Detection model	Precision	Recall	mAP@.5	mAP@.95
Original test set	Original	<u>0.836</u>	<u>0.512</u>	<u>0.523</u>	<u>0.400</u>
	Fine-tuned	0.828	0.499	0.512	0.396
Masked test set	Original	0.902	<u>0.582</u>	<u>0.607</u>	<u>0.476</u>
	Fine-tuned	<u>0.914</u>	0.551	0.595	0.469
Average	Original	0.869	<u>0.547</u>	<u>0.565</u>	<u>0.438</u>
	Fine-tuned	<u>0.871</u>	0.525	0.553	0.432

Table 6. Performance scores obtained by the original and fine-tuned YOLO object detectors on the original and masked test samples for **LIST** control. The average of performance scores on the original and masked test sets is reported as well. The best score between the original and fine-tuned models is shown in underlined face separately for original, masked, and average test results.

Test set	Detection model	Precision	Recall	mAP@.5	mAP@.95
Original test set	Original	<u>0.674</u>	<u>0.709</u>	<u>0.636</u>	<u>0.481</u>
	Fine-tuned	0.656	0.657	0.594	0.459
Masked test set	Original	0.592	0.516	0.414	0.301
	Fine-tuned	<u>0.783</u>	<u>0.734</u>	<u>0.737</u>	<u>0.609</u>
Average	Original	0.633	0.612	0.525	0.391
	Fine-tuned	<u>0.719</u>	<u>0.695</u>	<u>0.665</u>	<u>0.534</u>

Figure 11 shows an image from the user interface control detection test set with a mask on a TABLE control for which (a) the original YOLO detection model could not predict the correct boundaries of the control, and (b) the fine-tuned YOLO detection model correctly predicted the boundaries of the control. **Figure 12** shows another image from the user interface control detection test set with a mask on a TABLE control for which (a) the original YOLO detection model could not predict the correct boundaries of the control and detected two separate parts of it, and (b) the fine-tuned YOLO detection model predicted the correct boundary box of the control. There are many examples like these that demonstrate the effectiveness of our data augmentation

strategy using the local masks to enhance the accuracy of the object detection model in scenarios where some parts of controls are not visible.

Table 7. Performance scores obtained by the original and fine-tuned YOLO object detectors on the original and masked test samples for **TABBAR** control. The average of performance scores on the original and masked test sets is reported as well. The best score between the original and fine-tuned models is shown in underlined face separately for original, masked, and average test results.

Test set	Detection model	Precision	Recall	mAP@.5	mAP@.95
Original test set	Original	<u>0.905</u>	0.582	<u>0.645</u>	<u>0.562</u>
	Fine-tuned	0.882	<u>0.637</u>	0.635	0.544
Masked test set	Original	0.820	0.627	0.620	0.536
	Fine-tuned	<u>0.866</u>	<u>0.648</u>	<u>0.652</u>	<u>0.578</u>
Average	Original	0.862	0.604	0.632	0.549
	Fine-tuned	<u>0.874</u>	<u>0.642</u>	<u>0.643</u>	<u>0.561</u>

3.6.2. Airplane detection

Exploring the images for which the R-CNN model could not correctly predict bounding boxes, we found that the model made errors when airplanes were very close to each other and some parts of the bounding box around an airplane was covered by other airplanes in the images. Moreover, the object detector could not perform accurately when the shadow of an airplane appeared in the image. In order to investigate whether our data augmentation strategy can help to address these challenges, we randomly selected 100 images from the training set and applied the local masking technique. Ten different masked versions were generated for each of the images such that there was only one local mask in every masked image. We then fine-tuned the object detector on the combination of original training samples and new masked training images. We also created a new masked test set by randomly selecting 40 images from the original test samples, applying the local masking technique, and generating five different masked versions for every image.

As already mentioned in **Section 3.4**, the original R-CNN model obtained an accuracy of 87.05% on the original test set. It also obtained an accuracy of 82.5% on the masked test set. On the other hand, the fine-tuned model obtained an accuracy of 89.3% and 90.75% on the original and masked test sets, respectively. The average accuracy on both the original and masked test sets was 84.77% for the original model and 90.02% for the fine-tuned model. This shows that fine-tuning on the images resulted from our local masking method has a positive impact on improving the accuracy of the object detector on unmasked and masked images. This can be also helpful to

increase the robustness of the detection model when some parts of the target object are covered by other objects, or shadows in the image makes it difficult to detect the correct boundaries.

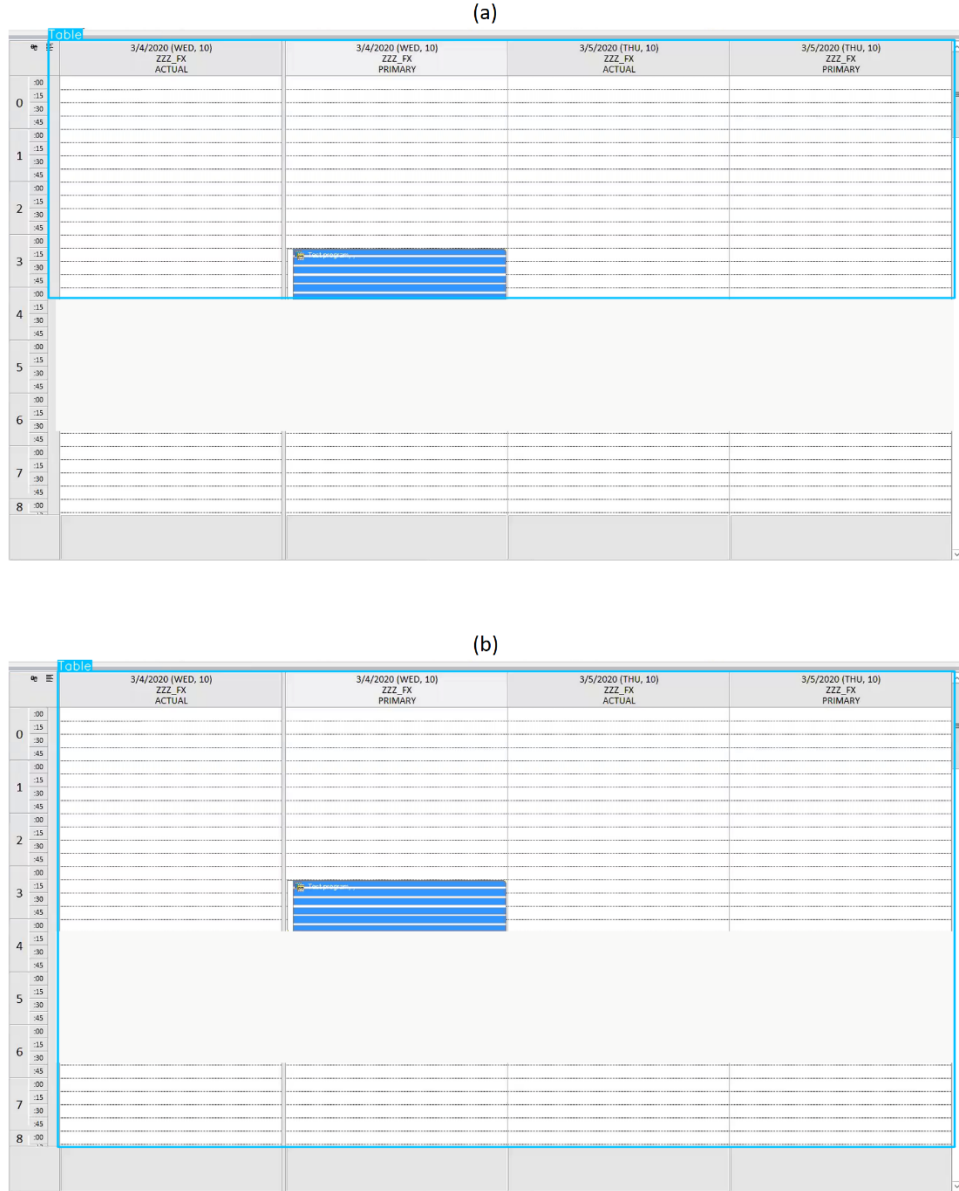


Figure 11. An image from the user interface control detection test set with a mask on a TABLE control for which (a) the original YOLO detection model could not predict the correct boundaries of the control, and (b) the fine-tuned YOLO detection model correctly predicted the boundaries of the control.

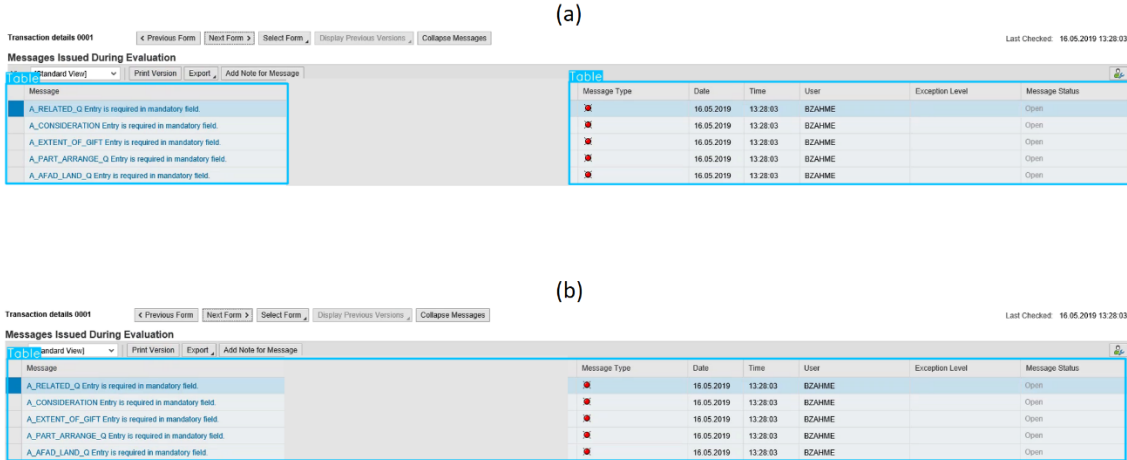


Figure 12. An image from the user interface control detection test set with a mask on a TABLE control for which (a) the original YOLO detection model could not predict the correct boundaries of the control and detected two separate parts of it, and (b) the fine-tuned YOLO detection model predicted the correct boundary box of the control.

3.6.3. Vehicle detection

Investigating those images for which the SSD object detector could not correctly predict bounding boxes, we found that the accuracy of object detection tended to decrease on images where there were overlap between bounding boxes of multiple objects, or some part of an object was covered by another object. We again utilized the local masking technique to generate samples for data augmentation, in order to examine how effective this method can be to cope with the aforementioned problem. We randomly selected 500 images from the training set, applied the local masking method, and generated eight different masked versions for every image. We then fine-tuned the SSD detection model on a combination of the original and masked training samples. We also created a new masked test set by randomly selecting 300 images from the original test samples, applying the local masking technique, and generating five different masked versions for every image.

Table 8 presents the performance scores obtained by the fine-tuned SSD model on the original vehicle detection test set. Compared to the scores reported for the original SSD model (trained on the original training images) in **Table 2**, the fine-tuned model performed slightly better on CAR and MOTORCYCLE objects and worse on BUS and TRUCK objects. The difference between the average scores on all the four classes obtained by the original and the fine-tuned models was such small that they can be considered almost equal.

The performance scores of the original and fine-tuned SSD model on the masked test set are reported in **Table 9**. As can be seen, the fine-tuned model was able to perform better over all the classes and performance measures. **Table 10** reports the average performance scores obtained by

the original and fine-tuned SSD models on both the original and masked vehicle detection test sets. As the results show, the fine-tuned model outperformed the original model with respect to all the classes and accuracy measures. Similar to what we discussed in **Section 3.6.1** and Section **3.6.2**, these results suggest that utilizing the local masking method and using the masked images for data augmentation can effectively improve the object detection performance and help the object detectors perform more robustly.

Table 8. The performance scores obtained by the fine-tuned SSD detection model on the original vehicle detection test set.

Class	Precision	Recall	mAP@.7
ALL	0.815	0.785	0.769
CAR	0.857	0.820	0.798
BUS	0.812	0.776	0.760
TRUCK	0.773	0.744	0.725
MOTORCYCLE	0.819	0.802	0.793

Table 9. The performance scores obtained by the original and fine-tuned SSD detection models on the masked vehicle detection test set. The best score between the original and fine-tuned models is shown in underlined face separately for each class and all classes.

Class	Detection model	Precision	Recall	mAP@.7
ALL	Original	0.770	0.744	0.716
	Fine-tuned	<u>0.833</u>	<u>0.806</u>	<u>0.787</u>
CAR	Original	0.812	0.775	0.736
	Fine-tuned	<u>0.881</u>	<u>0.839</u>	<u>0.813</u>
BUS	Original	0.781	0.757	0.729
	Fine-tuned	<u>0.827</u>	<u>0.794</u>	<u>0.785</u>
TRUCK	Original	0.738	0.720	0.703
	Fine-tuned	<u>0.785</u>	<u>0.761</u>	<u>0.733</u>
MOTORCYCLE	Original	0.752	0.725	0.696
	Fine-tuned	<u>0.840</u>	<u>0.830</u>	<u>0.817</u>

Table 10. The average performance scores obtained by the original and fine-tuned SSD detection models on both the original and masked vehicle detection test sets. The best score between the original and fine-tuned models is shown in underlined face separately for each class and all classes.

Class	Detection model	Precision	Recall	mAP@.7
ALL	Original	0.791	0.762	0.740
	Fine-tuned	<u>0.824</u>	<u>0.795</u>	<u>0.778</u>
CAR	Original	0.828	0.788	0.759
	Fine-tuned	<u>0.869</u>	<u>0.829</u>	<u>0.805</u>
BUS	Original	0.800	0.769	0.747
	Fine-tuned	<u>0.819</u>	<u>0.785</u>	<u>0.772</u>
TRUCK	Original	0.761	0.736	0.722
	Fine-tuned	<u>0.779</u>	<u>0.752</u>	<u>0.729</u>
MOTORCYCLE	Original	0.777	0.756	0.733
	Fine-tuned	<u>0.829</u>	<u>0.816</u>	<u>0.805</u>

4. Conclusion

In this paper, we proposed BODEM that is a method for explaining the output of object detection models in a black-box manner. Our explanation method uses local and global masks to cover different areas of an input image, and estimates the importance of those areas by measuring how the object detection model reacts to the masked images. We conducted extensive experiments on various object detection DL models and datasets. The experimentations showed that BODEM can be effectively used to generate visual explanations that reveal which parts of images and objects are more important when an object detector makes a decision. The explanations helped us find useful patterns about the behavior of detection models on different tasks and objects. The explanation method does not need to have access to the underlying ML model's internals or any other information about its structure or settings. This makes BODEM a proper choice for explaining and validating the behavior of object detection systems and reveal their vulnerabilities in black-box software testing scenarios. It was already investigated how failure points of natural language processing deep learning models can be revealed by injecting small amounts of noise into the input and observing changes in the behavior of the models (Moradi & Samwald, 2021a).

We also utilized the local masking method of BODEM to generate masked images for data augmentation experiments. Fine-tuning the object detection models on a combination of masked

and clean images, we improved the performance of the detection models. The object detectors generally performed better on masked and clean images after they were fine-tuned. This demonstrated that locally masked images produced by BODEM can be effectively used to augment training data, and enhance the detection accuracy and robustness of the models.

Future research may address the expansion of BODEM to explanation methods for other computer vision tasks such as classification or segmentation.

References

Adadi, A., & Berrada, M. (2018). Peeking Inside the Black-Box: A Survey on Explainable Artificial Intelligence (XAI). *IEEE Access*, 6, 52138-52160. doi: <https://doi.org/10.1109/ACCESS.2018.2870052>

Bach, S., Binder, A., Montavon, G., Klauschen, F., Müller, K.-R., & Samek, W. (2015). On Pixel-Wise Explanations for Non-Linear Classifier Decisions by Layer-Wise Relevance Propagation. *PLOS ONE*, 10(7), e0130140. doi: <https://doi.org/10.1371/journal.pone.0130140>

Fong, R. C., & Vedaldi, A. (2017). *Interpretable explanations of black boxes by meaningful perturbation*. Paper presented at the Proceedings of the IEEE International Conference on Computer Vision.

Freitas, A. A. (2014). Comprehensible classification models: a position paper. *SIGKDD Explor. Newsl.*, 15(1), 1–10. doi: 10.1145/2594473.2594475

Girshick, R. (2015). *Fast r-cnn*. Paper presented at the Proceedings of the IEEE international conference on computer vision.

Girshick, R., Donahue, J., Darrell, T., & Malik, J. (2014). *Rich feature hierarchies for accurate object detection and semantic segmentation*. Paper presented at the Proceedings of the IEEE conference on computer vision and pattern recognition.

Gu, J., Wang, Z., Kuen, J., Ma, L., Shahroudy, A., Shuai, B., . . . Chen, T. (2018). Recent advances in convolutional neural networks. *Pattern Recognition*, 77, 354-377. doi: <https://doi.org/10.1016/j.patcog.2017.10.013>

Guidotti, R., Monreale, A., Ruggieri, S., Turini, F., Giannotti, F., & Pedreschi, D. (2018). A Survey of Methods for Explaining Black Box Models. *ACM Comput. Surv.*, 51(5), 1-42. doi: <https://doi.org/10.1145/3236009>

He, K., Gkioxari, G., Dollár, P., & Girshick, R. (2017). *Mask r-cnn*. Paper presented at the Proceedings of the IEEE international conference on computer vision.

Jiao, L., Zhang, F., Liu, F., Yang, S., Li, L., Feng, Z., & Qu, R. (2019). A Survey of Deep Learning-Based Object Detection. *IEEE Access*, 7, 128837-128868. doi: 10.1109/ACCESS.2019.2939201

Khamparia, A., & Singh, K. M. (2019). A systematic review on deep learning architectures and applications. *Expert Systems*, 36(3), e12400. doi: <https://doi.org/10.1111/exsy.12400>

LeCun, Y., Bengio, Y., & Hinton, G. (2015). Deep learning. *Nature*, 521(7553), 436-444. doi: <https://doi.org/10.1038/nature14539>

Lin, T.-Y., Maire, M., Belongie, S., Hays, J., Perona, P., Ramanan, D., . . . Zitnick, C. L. (2014). *Microsoft COCO: Common Objects in Context*, Cham.

Liu, W., Anguelov, D., Erhan, D., Szegedy, C., Reed, S., Fu, C.-Y., & Berg, A. C. (2016). *SSD: Single Shot MultiBox Detector*, Cham.

Liu, W., Wang, Z., Liu, X., Zeng, N., Liu, Y., & Alsaadi, F. E. (2017). A survey of deep neural network architectures and their applications. *Neurocomputing*, 234, 11-26. doi: <https://doi.org/10.1016/j.neucom.2016.12.038>

Montavon, G., Lapuschkin, S., Binder, A., Samek, W., & Müller, K.-R. (2017). Explaining nonlinear classification decisions with deep Taylor decomposition. *Pattern Recognition*, 65, 211-222. doi: <https://doi.org/10.1016/j.patcog.2016.11.008>

Moradi, M., & Samwald, M. (2021a). *Evaluating the Robustness of Neural Language Models to Input Perturbations*, Online and Punta Cana, Dominican Republic.

Moradi, M., & Samwald, M. (2021b). Explaining Black-Box Models for Biomedical Text Classification. *IEEE Journal of Biomedical and Health Informatics*, 25(8), 3112-3120. doi: <https://doi.org/10.1109/JBHI.2021.3056748>

Moradi, M., & Samwald, M. (2021c). Post-hoc explanation of black-box classifiers using confident itemsets. *Expert Systems with Applications*, 165, 113941. doi: <https://doi.org/10.1016/j.eswa.2020.113941>

Moradi, M., & Samwald, M. (2022a). Deep Learning, Natural Language Processing, and Explainable Artificial Intelligence in the Biomedical Domain. *arXiv preprint arXiv:2202.12678*.

Moradi, M., & Samwald, M. (2022b). Improving the robustness and accuracy of biomedical language models through adversarial training. *Journal of Biomedical Informatics*, 132, 104114. doi: <https://doi.org/10.1016/j.jbi.2022.104114>

Murdoch, W. J., Singh, C., Kumbier, K., Abbasi-Asl, R., & Yu, B. (2019). Interpretable machine learning: definitions, methods, and applications. *arXiv preprint arXiv:1901.04592*.

Nguyen, A., Dosovitskiy, A., Yosinski, J., Brox, T., & Clune, J. (2016). *Synthesizing the preferred inputs for neurons in neural networks via deep generator networks*. Paper presented at the Advances in neural information processing systems.

Petsiuk, V., Das, A., & Saenko, K. (2018). *RISE: Randomized input sampling for explanation of black-box models*. Paper presented at the the British Machine Vision Conference (BMVC).

Petsiuk, V., Jain, R., Manjunatha, V., Morariu, V. I., Mehra, A., Ordonez, V., & Saenko, K. (2021). *Black-box explanation of object detectors via saliency maps*. Paper presented at the Proceedings of the IEEE/CVF Conference on Computer Vision and Pattern Recognition.

Redmon, J., Divvala, S., Girshick, R., & Farhadi, A. (2016). *You only look once: Unified, real-time object detection*. Paper presented at the Proceedings of the IEEE conference on computer vision and pattern recognition.

Ren, S., He, K., Girshick, R., & Sun, J. (2015). Faster r-cnn: Towards real-time object detection with region proposal networks. *Advances in neural information processing systems*, 28.

Ribeiro, M. T., Singh, S., & Guestrin, C. (2016). *"Why Should I Trust You?": Explaining the Predictions of Any Classifier*. Paper presented at the Proceedings of the 22nd ACM SIGKDD International Conference on Knowledge Discovery and Data Mining, San Francisco, California, USA.

Zaidi, S. S. A., Ansari, M. S., Aslam, A., Kanwal, N., Asghar, M., & Lee, B. (2022). A survey of modern deep learning based object detection models. *Digital Signal Processing*, 126, 103514. doi: <https://doi.org/10.1016/j.dsp.2022.103514>

Zhao, Z. Q., Zheng, P., Xu, S. T., & Wu, X. (2019). Object Detection With Deep Learning: A Review. *IEEE Transactions on Neural Networks and Learning Systems*, 30(11), 3212-3232. doi: [10.1109/TNNLS.2018.2876865](https://doi.org/10.1109/TNNLS.2018.2876865)

Zintgraf, L. M., Cohen, T. S., Adel, T., & Welling, M. (2017). Visualizing deep neural network decisions: Prediction difference analysis. *arXiv preprint arXiv:1702.04595*.